Synthesis of Inductive Power Transfer Converters With Dual Immittance Networks for Inherent CC-to-CV Charging Profiles

Zhicong Huang, *Senior Member, IEEE*, Tian Qin, *Student Member, IEEE*, Xiaolu Lucia Li, *Member, IEEE*, Li Ding, *Member, IEEE*, Herbert Ho-Ching Iu, *Senior Member, IEEE*, and Chi K. Tse, *Fellow, IEEE*

***Abstract*—To comply with the constant current (CC) and constant voltage (CV) charging characteristics of a lithium battery, it is expected that an inductive power transfer (IPT) charging system can provide the required power forms simultaneously. This article first proposes a systematic design pathway for IPT charging systems that inherently support CC-to-CV charging profiles on the basis of immittance networks. By appropriately connecting an IPT immittance network and a clamping immittance network with resistive input impedance and constant output characteristics, a family of IPT charging systems capable of delivering CC and CV output forms can be derived. Restricting the number of the compensation components to a maximum of 4, a total of 11 types of IPT immittance networks and six types of clamping immittance networks are derived. These immittance networks can be combined in various ways to provide 11×6 possible inherent CC-to-CV charging systems. The inherent CC-to-CV transition capability under passive control is achieved, maximizing the simplicity of control schemes. Both the design freedom for parameter configuration and the modularity of charging systems are improved, due to the power decoupling nature of the interconnected dual immittance networks. Two sets of IPT battery chargers are constructed to verify the proposed design methodology.**

***Index Terms*—Battery charging, constant current (CC), constant voltage (CV), inductive power transfer (IPT), passive solution.**

I. Introduction

INDUCTIVE power transfer (IPT) technology has emerged as a promising trend for future power supply, due to its superior safety coefficient, enhanced flexibility and convenience, and ease of automation compared with traditional conductive charging methods [1], [2]. The successful application of IPT technology has been demonstrated in numerous scenarios, including electric vehicles [3], [4], [5], biomedicine [6], [7], [8], and consumer electronics [9], [10], among others.

Lithium-ion batteries, being a relatively new and high-performance battery technology, have generated substantial interest and found widespread application across various industries. To fully maximize the advantages of these batteries, careful consideration of an appropriate charging method is essential. Conventionally, lithium-ion battery charging requires the usage of charging methods featuring constant current (CC) and constant voltage (CV) characteristics [11]. As such, IPT transfer technology has been extensively studied and applied to meet this requirement, necessitating the tackling of technical challenges to achieve both CC and CV output forms with a single IPT system [12], [13].

Multiple approaches have been proposed, aiming to address the challenges mentioned above. An intuitive approach to achieve both CC and CV output forms with a single IPT system is through incorporating a dc–dc converter at the secondary side, which regulates the output current and voltage [14], [15]. However, the addition of a dc–dc converter as an extra stage increases design complexity, raises component cost, and degrades system efficiency. To minimize the power stage of the charging system, further research in the manner of control development and topology modification is then conducted. It is possible to utilize an active rectifier instead of the traditional passive rectifier to perform the functions typically carried out by a dc–dc converter. Nevertheless, this substitution leads to a more intricate control scheme, as it necessitates the inclusion of extra design for detection, calculation, and communication, as presented in the previous work [16], [17]. To simplify the control design, a primary-tuning IPT charging system adopting a switch-controlled capacitor is designed featuring no secondary-side control and wireless communication [18]. The primary tuning is achieved through the phase-shift modulation of the switch-controlled capacitor, while it is still necessary to detect the zero crossing point and amplitude of the primary tank circuit current for performing the modulation effectively. Frequency-hopping approaches, adjusting the operating frequency of an IPT system

Manuscript received 4 December 2023; revised 25 February 2024; accepted 22 March 2024. Date of publication 27 March 2024; date of current version 19 April 2024. This work is supported in part by the National Natural Science Foundation of China under Grant 52007067, in part by the Science and Technology Planning Project of Guangdong Province under Grant 2023A0505050124, in part by the Natural Science Foundation of Guangdong Province under Grant 2023A1515011623, and in part by Hong Kong RGC Theme-Based Research Scheme Project under Grant T23-701/20R. Recommended for publication by Associate Editor M. Ponce-Silva. *(Corresponding authors: Zhicong Huang; Xiaolu Lucia Li.)*

Zhicong Huang and Tian Qin are with the Shien-Ming Wu School of Intelligent Engineering, South China University of Technology, Guangzhou 510006, China (e-mail: zhiconghuang@scut.edu.cn; witianqin@mail.scut.edu.cn).

Xiaolu Lucia Li, Li Ding, and Chi K. Tse are with the Department of Electrical Engineering, City University of Hong Kong, Hong Kong, China (e-mail: luciali@ieee.org; lding27@cityu.edu.hk; cktse@ieee.org).

Herbert Ho-Ching Iu is with the School of Electrical, Electronics and Computer Engineering, University of Western Australia, Crawley, WA 6009, Australia (e-mail: herbert.iu@uwa.edu.au).

Color versions of one or more figures in this article are available at https://doi.org/10.1109/TPEL.2024.3382112.

Digital Object Identifier 10.1109/TPEL.2024.3382112

0885-8993 © 2024 IEEE. Personal use is permitted, but republication/redistribution requires IEEE permission.
See https://www.ieee.org/publications/rights/index.html for more information.

Authorized licensed use limited to: SOUTH CHINA UNIVERSITY OF TECHNOLOGY. Downloaded on May 14,2024 at 07:30:27 UTC from IEEE Xplore. Restrictions apply.

TABLE I
COMPARISON WITH EXISTING DESIGNS

Desirable features	Backend converter [14], [15]	Active rectifiers [16], [17]	Switch-controlled capacitor [18]	Frequency hopping [4],[19]-[23]	Hybrid switching [28]-[32]	Proposed scheme
No control/sensing	×	×	×	×	×	√
No wireless feedback	√	√	×	×	possible	√
Fixed frequency	√	√	√	×	√	√
Simplified secondary design	×	×	Possible	Possible	Possible	Possible
Add-on cost	DC/DC converter	Active switches	Active switches	Unnecessary	Bidirectional switches	Resonant tank and rectifier

from the CC point to the CV point, ease the control efforts further [4], [19], [20]. However, the bifurcation phenomenon can be caused by large frequency variation [21], [22], [23]. Besides, the parameter configuration and frequency calculation process for frequency-hopping methods tend to be relatively complex.

In addition to the second-order compensation circuits that enable CC or CV output, higher order compensation circuits that support CC or CV output are also studied [24], [25], [26], [27]. These compensation circuits are utilized to mitigate the impact introduced due to frequency variation. Hybrid compensation structures are derived by combining two sets of compensation circuits, with each set enabling CC output and CV output, respectively, at the same operating frequency. By selectively switching between these different topological networks using ON/OFF control of the switches, both CC and CV output forms can be provided with a single system [28], [29], [30], [31], [32]. Despite the significant reduction in control complexity and complete elimination of frequency variation, the use of ac switches in this type of topological modification is inevitable. Consequently, active control techniques for topology switching, along with detection methods for output states, are still necessary, particularly in the context of battery charging that requires CC-to-CV transition. Furthermore, during the design process, it is necessary to consider at least two sets of compensation networks and ensure seamless interaction between these sets, which complicates the parameter configuration.

According to the aforementioned development, it remains a challenge to achieve both a simple design of control scheme and a straightforward configuration of topology parameter. In this article, therefore, we try to systematically address this issue by exploring the design pathway of IPT systems that possess the capability of automatic CC-to-CV transition and offer high freedom for topology parameter selection. The design starts with immittance networks, which are composed of capacitors and/or inductors. An immittance network can be viewed as a two-port network, which converts a voltage source into a current source, and vice versa, as long as the input impedance is proportional to the load admittance connected to the output [33]. It has been investigated that power flow between each energy port can be easily controlled by connecting an independent current source to the voltage bus or an independent voltage source to the current bus, thus easily achieving the bidirectional and decoupling power control of each energy port and facilitating the implementation of zero voltage switching [34]. Following this connection style, we suggest the series connection of a clamping immittance network with the IPT immittance network. Such a configuration enables the automatic CC-to-CV charging process and removes the requirement of communication between the primary and secondary sides, which maximizes the simplicity of control. Moreover, the power decoupling feature between immittance networks streamlines the parameter process, enhancing the design freedom and improving the system modularity. Since approximate zero reactive power can also be achieved, reactive power circulation and power losses can be eased. Table I summarizes the desired features of an IPT charging system and compares the proposed scheme with existing schemes. The proposed scheme features all the desired features, and as a pure passive scheme, it can eliminate complex sensing, active control, and wireless feedback, and it also enables a simple secondary design.

The rest of this article is organized as follows. Section II analyzes the characteristics of an immittance network. On this basis, the configuration of an IPT system with inherent CC-to-CV transition consisting of an IPT immittance network and a clamping immittance network is designed. The corresponding operating principles are also described. Section III identifies available IPT immittance networks and clamping immittance networks. Configuration requirements of the networks are then presented, providing the selection guidelines of appropriate structures in different application scenarios. Experimental results are given in Section IV. Finally, Section V concludes this article.

II. SYSTEM CONFIGURATION AND ANALYSIS

A. Characteristics of Immittance Network

A resonant circuit can be considered as a two-port network, as shown by Fig. 1(a). The voltages and currents at the primary and the secondary ports are sinusoidal and represented by $\mathbf{V}_1$, $\mathbf{I}_1$, $\mathbf{V}_2$, and $\mathbf{I}_2$, respectively. The two-port network can be defined as an immittance network [33], if its circuit equations satisfy

$$\begin{bmatrix}\mathbf{V}_1\\ \mathbf{I}_1\end{bmatrix}=\begin{bmatrix}0 & jZ_0\\ j\frac{1}{Z_0} & 0\end{bmatrix}\begin{bmatrix}\mathbf{V}_2\\ \mathbf{I}_2\end{bmatrix} \tag{1}$$

where Z_0 is defined as the characteristic impedance of the immittance network. Suppose the primary port is driven by a power source, and the output current and voltage at the secondary port can be derived as

$$\mathbf{I}_2=\frac{\mathbf{V}_1}{jZ_0}, \text{ and} \tag{2}$$

$$\mathbf{V}_2=-jZ_0\mathbf{I}_1 \tag{3}$$

Authorized licensed use limited to: SOUTH CHINA UNIVERSITY OF TECHNOLOGY. Downloaded on May 14,2024 at 07:30:27 UTC from IEEE Xplore. Restrictions apply.

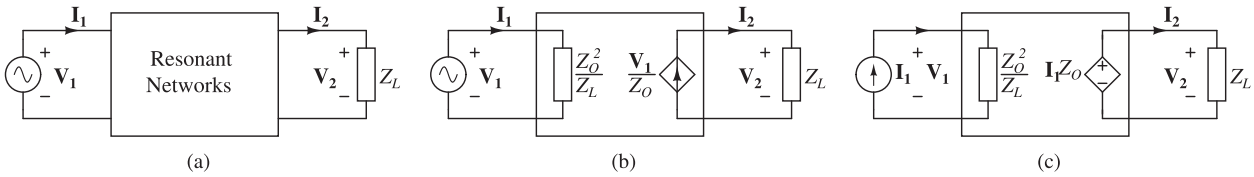

Fig. 1. Characteristics of resonant immittance network: (a) two-port network model, (b) CC output with CV input, and (c) CV output with CC input.

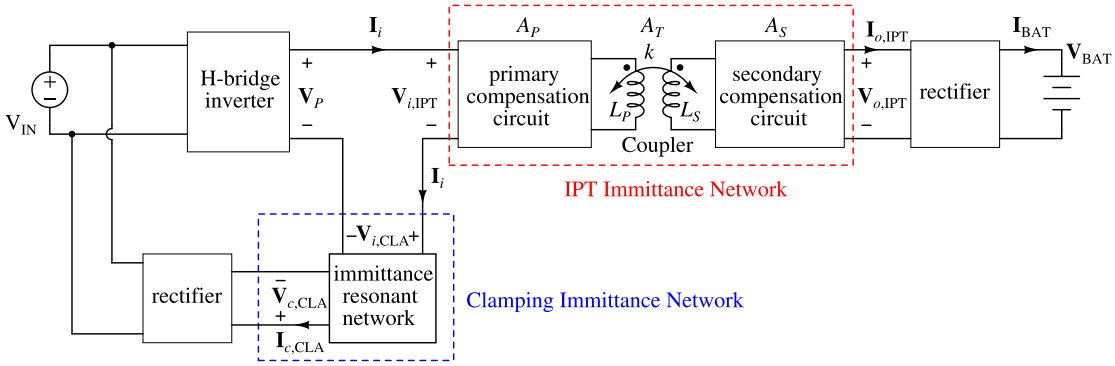

Fig. 2. Block diagram of the proposed IPT converters with dual immittance networks for inherent CC-to-CV charging profiles.

respectively. Given Z_L is the load impedance at the secondary port, it complies with

$$Z_L = \frac{\mathbf{V}_2}{\mathbf{I}_2}. \tag{4}$$

The input impedance of the immittance network, thus, can be derived as

$$Z_{\text{in}} = \frac{\mathbf{V}_1}{\mathbf{I}_1} = \frac{Z_0^2}{Z_L}. \tag{5}$$

With (2)–(5), some characteristics of the immittance network can be observed and concluded as follows.

1) It is noteworthy that the immittance network is reciprocal, which means either the primary or secondary port can be the input. When one port operates as the input, the other will be considered as the output.
2) From (2) and (3), the output current is proportional to the input voltage, and meanwhile, the output voltage is proportional to the input current. If the immittance network is driven by a source with a CV output, a CC output can be achieved, as shown in Fig. 1(b). Vice versa, if the immittance network is driven by a source with a CC output, a CV output can be achieved, as shown in Fig. 1(c).
3) From (5), unity power factor at the input port can be obtained, if the load is purely resistive, i.e. $Z_L = \Re(Z_L)$.

The abovementioned characteristics of immittance networks are utilized in this article to configure IPT systems featuring inherent CC-to-CV charging profiles and unity power factor.

B. System Configuration

Fig. 2 depicts the configuration of the proposed IPT systems that feature inherent CC-to-CV charging profiles and unity power factor. It includes two immittance networks, which are named as "*IPT Immittance Network*" and "*Clamping Immittance Network*" according to the functionality. The primary ports of these two immittance networks are in series connection and driven by a sinusoidal ac voltage source $\mathbf{V}_P$ chopped from a dc voltage source V_{IN}. With fundamental approximation, the amplitude of $\mathbf{V}_P$ is given by $|\mathbf{V}_P| = \frac{4}{\pi} V_{\text{IN}}$. Since these two immittance networks are in series connection, and thus, they share an identical primary current $\mathbf{I}_i$, whereas their primary voltages are donated as $\mathbf{V}_{i,\text{IPT}}$ and $\mathbf{V}_{i,\text{CLA}}$, respectively. Unless specified, subscripts "IPT" and "CLA" indicate associated parameters of the IPT immittance network and the clamping immittance network, respectively.

The secondary port of the clamping immittance network is rectified and then clamped by V_{IN}. Its voltage and current are given by $\mathbf{V}_{c,\text{CLA}}$ and $\mathbf{I}_{c,\text{CLA}}$, respectively. The secondary port of the IPT immittance network is rectified as a dc output to charge the battery. In the steady state, the battery can be modeled as a resistor given by $R_{\text{BAT}} = \frac{V_{\text{BAT}}}{I_{\text{BAT}}}$, where V_{BAT} and I_{BAT} are the battery terminal voltage and the charging current, respectively. The equivalent load at the secondary port of the IPT immittance network is given by $R_{\text{eq}} = \beta R_{\text{BAT}}$, where β is a scaling factor determined by the filter used in the rectifier [35]. To be specific, if the secondary compensation circuit includes a component in series connection with the rectifier circuit, a capacitor filter should be used and $\beta = \frac{8}{\pi^2}$. If the secondary compensation circuit includes a component in parallel connection with the rectifier circuit, an inductor filter should be used and $\beta = \frac{\pi^2}{8}$. The voltage and current at the secondary port of the IPT immittance network are $\mathbf{V}_{o,\text{IPT}}$ and $\mathbf{I}_{o,\text{IPT}}$, and they are in phase complying with $R_{\text{eq}} = \frac{\mathbf{V}_{o,\text{IPT}}}{\mathbf{I}_{o,\text{IPT}}}$.

As shown in Fig. 2, the IPT immittance network is responsible for wireless power transfer, and it consists of a primary

Authorized licensed use limited to: SOUTH CHINA UNIVERSITY OF TECHNOLOGY. Downloaded on May 14,2024 at 07:30:27 UTC from IEEE Xplore. Restrictions apply.

compensation circuit, a loosely coupled transformer, and a secondary compensation circuit, which are cascaded in series. All these three parts can be represented by 2×2 transmission metrics, given by A_P, A_T, and A_S, respectively. To be an immittance network, the overall transmission matrix should satisfy (1) and, thus, can be given by

$$A_{\mathrm{IPT}} = A_P A_T A_S = \begin{bmatrix} 0 & jZ_{0,\mathrm{IPT}} \\ j\frac{1}{Z_{0,\mathrm{IPT}}} & 0 \end{bmatrix} \tag{6}$$

where $Z_{0,\mathrm{IPT}}$ is the characteristic impedance of the IPT immittance network. The circuit equations of the IPT immittance network are given by

$$[\mathbf{V}_{i,\mathrm{IPT}}, \mathbf{I}_i]^T = A_{\mathrm{IPT}} [\mathbf{V}_{o,\mathrm{IPT}}, \mathbf{I}_{o,\mathrm{IPT}}]^T. \tag{7}$$

Similarly, the clamping immittance network is a resonant circuit with circuit equations satisfying (1), and thus, its transmission matrix is given by

$$A_{\mathrm{CLA}} = \begin{bmatrix} 0 & jZ_{0,\mathrm{CLA}} \\ j\frac{1}{Z_{0,\mathrm{CLA}}} & 0 \end{bmatrix} \tag{8}$$

where $Z_{0,\mathrm{CLA}}$ is the characteristic impedance of the clamping immittance network. The circuit equations of the clamping immittance network are given by

$$[\mathbf{V}_{i,\mathrm{CLA}}, \mathbf{I}_i]^T = A_{\mathrm{CLA}} [\mathbf{V}_{c,\mathrm{CLA}}, \mathbf{I}_{c,\mathrm{CLA}}]^T. \tag{9}$$

C. Operating Principle

With fundamental approximation, all voltages and currents at the ports of the immittance networks in Fig. 2 are considered as sinusoidal. Ideally, there are two operating modes: CC mode and CV mode. In the CC mode, the secondary port of the clamping immittance network ($\mathbf{V}_{c,\mathrm{CLA}}$) is unclamped due to the reverse bias of the rectifier, whereas in the CV mode, it is clamped by the voltage source V_{IN} due to the fully conducted rectifier. A detailed illustration is given as follows.

1) CC Mode: Based on the analysis in Sections II-A and II-B, the IPT immittance network can achieve a CC output if it is driven by a CV source. Note that the secondary port of the clamping immittance network is unclamped and open circuit (∞), if the rectifier is reverse biased, i.e.,

$$|\mathbf{V}_{c,\mathrm{CLA}}| \le V_{\mathrm{IN}}. \tag{10}$$

Thus, with (5), the primary port of the clamping immittance network has null input impedance and can be considered as short-circuit, i.e.,

$$\mathbf{V}_{i,\mathrm{CLA}} = 0. \tag{11}$$

In this case, the IPT immittance network is driven by a CV source as given by (12). According to (6) and (7), it can achieve a CC output as given by (13)

$$\mathbf{V}_{i,\mathrm{IPT}} = \mathbf{V}_P \tag{12}$$

$$\mathbf{I}_{o,\mathrm{IPT}} = \frac{\mathbf{V}_P}{jZ_{0,\mathrm{IPT}}}. \tag{13}$$

Since the load at the secondary port of the IPT immittance network is purely resistive, i.e., $\mathbf{V}_{o,\mathrm{IPT}}$ and $\mathbf{I}_{o,\mathrm{IPT}}$ are in phase, unity power factor can be achieved at the primary port of the IPT immittance network with (5). It also holds true for the overall IPT system.

Observed from the primary port, the clamping immittance network is driven by $\mathbf{I}_i$, which depends on the load condition. With (5) and (12), it can be derived as

$$\mathbf{I}_i = \frac{\mathbf{V}_P}{Z_{0,\mathrm{IPT}}^2} R_{\mathrm{eq}}. \tag{14}$$

Excited by $\mathbf{I}_i$ at the primary port, the voltage at the secondary port of the clamping immittance network can be derived with (8) and (9) and is given by

$$\mathbf{V}_{c,\mathrm{CLA}} = -jZ_{0,\mathrm{CLA}}\mathbf{I}_i = \frac{-jZ_{0,\mathrm{CLA}}\mathbf{V}_P R_{\mathrm{eq}}}{Z_{0,\mathrm{IPT}}^2}. \tag{15}$$

To satisfy the assumption given in (10), the range of R_{eq} can be derived as

$$0 < R_{\mathrm{eq}} \le \frac{Z_{0,\mathrm{IPT}}^2}{\frac{4}{\pi} Z_{0,\mathrm{CLA}}}, \text{ for CC mode.} \tag{16}$$

2) CV Mode: Based on the analysis in Sections II-A and II-B, the IPT immittance network can provide a CV output if it is driven by a CC source. To achieve that, the clamping immittance network is designed to help with facilitating the CC source. If the rectifier is fully conducted, the secondary port of the clamping immittance network will be clamped as

$$|\mathbf{V}_{c,\mathrm{CLA,max}}| = \frac{4}{\pi} V_{\mathrm{IN}}. \tag{17}$$

It is observed that the clamping immittance network is driven by a CV source at the secondary port. Due to the characteristics of an immittance network described by (2), the current at its primary port is restricted to be constant. Thus, the current flowing through the primary port of the IPT immittance network is kept constant as given by

$$\mathbf{I}_i = \frac{\mathbf{V}_{c,\mathrm{CLA,max}}}{-jZ_{0,\mathrm{CLA}}}. \tag{18}$$

Driven by the CC source given in (18), the CV output at the secondary port of the IPT immittance network is derived as

$$\mathbf{V}_{o,\mathrm{IPT}} = \frac{Z_{0,\mathrm{IPT}}}{Z_{0,\mathrm{CLA}}} \mathbf{V}_{c,\mathrm{CLA,max}}. \tag{19}$$

The rectifier of the clamping immittance network is assumed to be fully conducted in (17), which means that the power is fed back to the source via the clamping immittance network, and the voltage at the primary port is not zero. Thus, the condition for (17) is

$$|\mathbf{V}_{i,\mathrm{IPT}}| < |\mathbf{V}_P|. \tag{20}$$

With (5) and (18), the voltage at the primary port of the IPT immittance network is given by

$$\mathbf{V}_{i,\mathrm{IPT}} = \frac{Z_{0,\mathrm{IPT}}^2 \mathbf{V}_{c,\mathrm{CLA}}}{-jZ_{0,\mathrm{CLA}} R_{\mathrm{eq}}}. \tag{21}$$

Authorized licensed use limited to: SOUTH CHINA UNIVERSITY OF TECHNOLOGY. Downloaded on May 14,2024 at 07:30:27 UTC from IEEE Xplore. Restrictions apply.

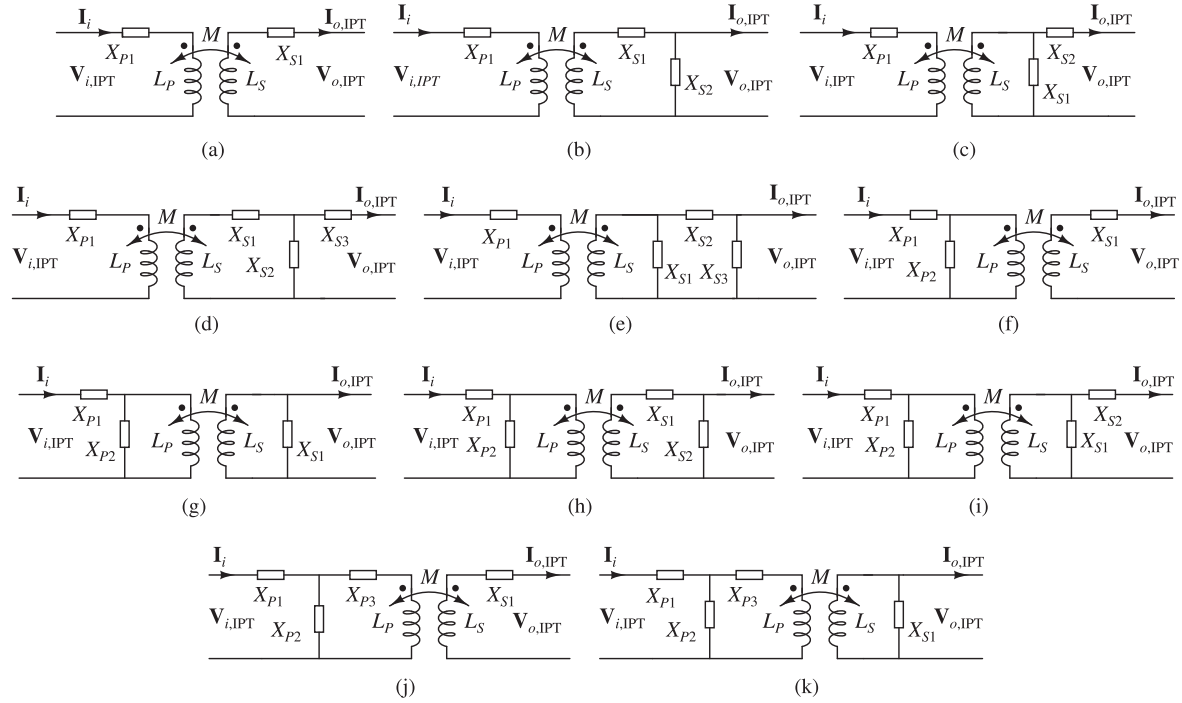

Fig. 3. Available IPT immittance networks with up to four compensation components. (a) S-S. (b) S-SP. (c) S-PS. (d) S-T. (e) S-Π. (f) SP-S. (g) SP-P. (h) SP-SP. (i) SP-PS. (j) T-S. (k) T-P.

Therefore, the range of $R_{\rm eq}$ for CV mode can be derived as

$$R_{\rm eq} \geq \frac{Z_{0,\rm IPT}^2}{Z_{0,\rm CLA}}, \text{ for CV mode.} \tag{22}$$

The input impedances at the primary ports of both immittance networks are resistive, because the corresponding voltages and currents at both secondary ports are in phase. Therefore, unity power factor can be achieved at the input of the overall system.

In addition, it can be estimated from (16) and (22) that there is a narrow transition process from the CC mode to CV mode in practice, i.e., $R_{\rm eq} \in \left(\frac{Z_{0,\rm IPT}^2}{\frac{4}{\pi}Z_{0,\rm CLA}}, \frac{Z_{0,\rm IPT}^2}{Z_{0,\rm CLA}}\right]$, which is caused by the nonlinearity of the rectifier (partial conduction) in the clamping circuit. Nevertheless, it will not affect the realization of inherent CC-to-CV charging profiles.

III. Available Circuit Topologies

A. IPT Immittance Networks

As illustrated in Section II-B, the IPT resonant tank consists of three components: the loosely coupled transformer, the primary compensation circuit, and the secondary compensation circuit. The IPT resonant tank is designed to provide CC output when the corresponding input is a CV source. Meanwhile, it is capable of delivering CV output when the corresponding input is a CC source, given its design fulfills the requirements of the immittance network, i.e., its transmission matrix satisfies (1).

In general, the transmission matrix of the loosely coupled transformer A_T can be represented as

$$A_T = \begin{bmatrix} \frac{L_P}{M} & j\omega M\left(\frac{1}{k^2}-1\right) \\ \frac{1}{j\omega M} & \frac{L_S}{M} \end{bmatrix} \tag{23}$$

where L_P, L_S, and M are the primary self-inductance, secondary self-inductance, and mutual inductance, respectively. As usual, k is the coupling coefficient given by $k = \frac{M}{\sqrt{L_P L_S}}$. According to (23), it is obvious that the loosely coupled transformer is not an immittance network, and thus, the design of A_P and A_S for compensation is needed.

A variety of compensation circuit topologies together with appropriate parameters design are possible to facilitate IPT immittance networks. To simplify the deviation of compensation designs, the available topologies of IPT immittance networks with the maximum number of total components being restricted to four are depicted in Fig. 3. With the corresponding compensation designs summarized in the second column of Table II, the transmission matrix of the primary and secondary compensation circuits are given in the third column (A_P and A_S). In the same column, it can be observed that the overall IPT immittance networks $A_{\rm IPT}$ satisfy (12), which means the compensation designs enable immittance networks. The characteristic impedance of the IPT immittance network is donated as $Z_{0,\rm IPT}$.

B. Clamping Immittance Networks with Isolation

For the clamping immittance network, it is crucial to maintain electrical isolation from the IPT immittance network to prevent potential shoot-through issues in the inverter and rectifier within the primary circuit. Therefore, an isolated transformer with a 1:1 turn ratio is connected in cascade with the clamping immittance network, as shown in Fig. 4. Notably, the isolated transformer has no effect on the characteristics of the immittance network and its volume is minimized due to its closely coupled design.

Authorized licensed use limited to: SOUTH CHINA UNIVERSITY OF TECHNOLOGY. Downloaded on May 14,2024 at 07:30:27 UTC from IEEE Xplore. Restrictions apply.

TABLE II
AVAILABLE IPT IMMITTANCE NETWORKS

Topologies	Compensation design	IPT Networks	$Z_{0,\mathrm{IPT}}$
S-S	$X_{P1}=-X_{L_P}$ $X_{S1}=-X_{L_S}$	$A_P=\begin{bmatrix}1 & jX_{P1}\\ 0 & 1\end{bmatrix}$ $A_S=\begin{bmatrix}1 & jX_{S1}\\ 0 & 1\end{bmatrix}$ $A_{\mathrm{IPT}}=\begin{bmatrix}0 & -jX_M\\ \frac{1}{jX_M} & 0\end{bmatrix}$	$-X_M$
S-SP	$X_{S1}=-X_{L_S}$ $X_{S2}=\frac{{X_M}^2}{X_{L_P}+X_{P1}}$	$A_P=\begin{bmatrix}1 & jX_{P1}\\ 0 & 1\end{bmatrix}$ $A_S=\begin{bmatrix}\frac{X_{S1}+X_{S2}}{X_{S2}} & jX_{S1}\\ \frac{1}{jX_{S2}} & 1\end{bmatrix}$ $A_{\mathrm{IPT}}=\begin{bmatrix}0 & -jX_M\\ \frac{1}{jX_M} & 0\end{bmatrix}$	$-X_M$
S-PS	$X_{S1}=-X_{L_S}+\frac{{X_M}^2}{(X_{L_P}+X_{P1})}$ $X_{S2}=X_{L_S}(\frac{1}{k^2}-1)+\frac{X_{L_S}X_{P1}}{k^2X_{L_P}}$	$A_P=\begin{bmatrix}1 & jX_{P1}\\ 0 & 1\end{bmatrix}$ $A_S=\begin{bmatrix}1 & jX_{S2}\\ \frac{1}{jX_{S1}} & \frac{X_{S1}+X_{S2}}{X_{S1}}\end{bmatrix}$ $A_{\mathrm{IPT}}=\begin{bmatrix}0 & \frac{j[X_{L_P}X_{L_S}(1-k^2)+X_{L_S}X_{P1}]}{X_M}\\ \frac{jX_M}{X_{L_P}X_{L_S}(1-k^2)+X_{L_S}X_{P1}} & 0\end{bmatrix}$	$\frac{X_{L_P}X_{L_S}(1-k^2)+X_{L_S}X_{P1}}{X_M}$
S-T	$X_{S1}=\frac{{X_M}^2}{X_{L_P}+X_{P1}}-(X_{L_S}+X_{S2})$ $X_{S3}=\frac{{X_{S2}}^2(X_{L_P}+X_{P1})}{{X_M}^2}-X_{S2}$	$A_P=\begin{bmatrix}1 & jX_{P1}\\ 0 & 1\end{bmatrix}$ $A_S=\frac{1}{X_{S2}}\begin{bmatrix}X_{S1}+X_{S2} & j(X_{S1}X_{S2}+X_{S2}X_{S3}+X_{S3}X_{S1})\\ -j & X_{S2}+X_{S3}\end{bmatrix}$ $A_{\mathrm{IPT}}=\begin{bmatrix}0 & -\frac{j(X_{L_P}+X_{P1})X_{S2}}{X_M}\\ -\frac{jX_M}{(X_{L_P}+X_{P1})X_{S2}} & 0\end{bmatrix}$	$-\frac{(X_{L_P}+X_{P1})X_{S2}}{X_M}$
S-Π	$X_{S1}=-\frac{X_{L_S}X_{S2}}{X_{L_S}+X_{S2}}$ $X_{S3}=\frac{k^2{X_{S2}}^2X_{L_P}}{(1-k^2)X_{L_P}X_{L_S}-k^2X_{L_P}X_{S2}+X_{P1}X_{L_S}}$	$A_P=\begin{bmatrix}1 & jX_{P1}\\ 0 & 1\end{bmatrix}$ $A_S=\begin{bmatrix}\frac{X_{S2}+X_{S3}}{X_{S3}} & jX_{S2}\\ \frac{-j(X_{S1}+X_{S2}+X_{S3})}{X_{S1}X_{S3}} & \frac{X_{S1}+X_{S2}}{X_{S1}}\end{bmatrix}$ $A_{\mathrm{IPT}}=\begin{bmatrix}0 & \frac{jX_MX_{S2}}{X_{L_S}}\\ \frac{jX_{L_S}}{X_MX_{S2}} & 0\end{bmatrix}$	$\frac{X_MX_{S2}}{X_{L_S}}$
SP-S	$X_{P1}=X_{L_P}[\frac{1}{k^2}(1+\frac{X_{S1}}{X_{L_S}})-1]$ $X_{P2}=-X_{L_P}+\frac{{X_M}^2}{X_{L_S}+X_{S1}}$	$A_P=\begin{bmatrix}\frac{X_{P1}+X_{P2}}{X_{P2}} & jX_{P1}\\ \frac{1}{jX_{P2}} & 1\end{bmatrix}$ $A_S=\begin{bmatrix}1 & jX_{S1}\\ 0 & 1\end{bmatrix}$ $A_{\mathrm{IPT}}=\begin{bmatrix}0 & j\frac{X_{L_P}X_{L_S}(1-k^2)+X_{L_P}X_{S1}}{X_M}\\ \frac{jX_M}{X_{L_P}X_{L_S}(1-k^2)+X_{L_P}X_{S1}} & 0\end{bmatrix}$	$\frac{X_{L_P}X_{L_S}(1-k^2)+X_{L_P}X_{S1}}{X_M}$
SP-P	$X_{P1}=(\frac{1}{k^2}-1)[\frac{(1-k^2)X_{L_S}}{X_{S1}}+1]$ $X_{P2}=(k^2-1)X_{L_P}$	$A_P=\begin{bmatrix}\frac{X_{P1}+X_{P2}}{X_{P2}} & jX_{P1}\\ \frac{1}{jX_{P2}} & 1\end{bmatrix}$ $A_S=\begin{bmatrix}1 & 0\\ \frac{1}{jX_{S1}} & 1\end{bmatrix}$ $A_{\mathrm{IPT}}=\begin{bmatrix}0 & \frac{j[(1-k^2)X_{L_P}X_{L_S}]}{X_M}\\ \frac{jX_M}{(1-k^2)X_{L_P}X_{L_S}} & 0\end{bmatrix}$	$\frac{(1-k^2)X_{L_P}X_{L_S}}{X_M}$
SP-SP	$X_{P2}=-X_{L_P}+\frac{{X_M}^2}{X_{L_S}+X_{S1}}$ $X_{S2}=\frac{[{X_M}^2-X_{L_P}(X_{L_S}+X_{S1})]^2}{{X_M}^2(X_{L_P}+X_{P1})-{X_{L_P}}^2(X_{L_S}+X_{S1})}$	$A_P=\begin{bmatrix}\frac{X_{P1}+X_{P2}}{X_{P2}} & jX_{P1}\\ \frac{1}{jX_{P2}} & 1\end{bmatrix}$ $A_S=\begin{bmatrix}\frac{X_{S1}+X_{S2}}{X_{S2}} & jX_{S1}\\ \frac{1}{jX_{S2}} & 1\end{bmatrix}$ $A_{\mathrm{IPT}}=\begin{bmatrix}0 & j\frac{X_{L_P}X_{L_S}(1-k^2)+X_{L_P}X_{S1}}{X_M}\\ \frac{jX_M}{X_{L_P}X_{L_S}(1-k^2)+X_{L_P}X_{S1}} & 0\end{bmatrix}$	$\frac{X_{L_P}X_{L_S}(1-k^2)+X_{L_P}X_{S1}}{X_M}$
SP-PS	$X_r={X_M}^2(X_{S1}+X_{S2})-X_{L_P}[X_{S1}X_{S2}+X_{L_S}(X_{S1}+X_{S2})]$ $X_{P1}=X_r[\frac{1}{X_{S1}^2}(1-\frac{1}{k^2})-\frac{1}{k^2X_{L_S}X_{S1}}]$ $X_{P2}=\frac{X_r}{X_{S1}X_{S2}+X_{L_S}(X_{S1}+X_{S2})}$	$A_P=\begin{bmatrix}\frac{X_{P1}+X_{P2}}{X_{P2}} & jX_{P1}\\ \frac{1}{jX_{P2}} & 1\end{bmatrix}$ $A_S=\begin{bmatrix}1 & jX_{S2}\\ \frac{1}{jX_{S1}} & \frac{X_{S1}+X_{S2}}{X_{S1}}\end{bmatrix}$ $A_{\mathrm{IPT}}=\begin{bmatrix}0 & -\frac{jX_r}{X_MX_{S1}}\\ \frac{jX_MX_{S1}}{-X_r} & 0\end{bmatrix}$	$-\frac{X_r}{X_MX_{S1}}$
T-S	$X_{P1}=\frac{{X_{P2}}^2(X_{L_S}+X_{S1})}{{X_M}^2}-X_{P2}$ $X_{P3}=\frac{{X_M}^2}{X_{L_S}+X_{S1}}-(X_{L_P}+X_{P2})$	$A_P=\frac{1}{X_{P2}}\begin{bmatrix}X_{P1}+X_{P2} & j(X_{P1}X_{P2}+X_{P2}X_{P3}+X_{P3}X_{P1})\\ -j & X_{P2}+X_{P3}\end{bmatrix}$ $A_S=\begin{bmatrix}1 & jX_{S1}\\ 0 & 1\end{bmatrix}$ $A_{\mathrm{IPT}}=\begin{bmatrix}0 & -\frac{jX_{P2}(X_{L_S}+X_{S1})}{X_M}\\ -\frac{jX_M}{X_{P2}(X_{L_S}+X_{S1})} & 0\end{bmatrix}$	$-\frac{X_{P2}(X_{L_S}+X_{S1})}{X_M}$
T-P	$X_{P1}=\frac{X_{P2}^2(X_{L_S}+X_{S1})}{k^2X_{L_P}X_{S1}}-X_{P2}$ $X_{P3}=(k^2-1)X_{L_P}-X_{P2}$	$A_P=\frac{1}{X_{P2}}\begin{bmatrix}X_{P1}+X_{P2} & j(X_{P1}X_{P2}+X_{P2}X_{P3}+X_{P3}X_{P1})\\ -j & X_{P2}+X_{P3}\end{bmatrix}$ $A_S=\begin{bmatrix}1 & 0\\ \frac{1}{jX_{S1}} & 1\end{bmatrix}$ $A_{\mathrm{IPT}}=\begin{bmatrix}0 & -\frac{jX_{L_S}X_{P2}}{X_M}\\ -\frac{jX_M}{X_{L_S}X_{P2}} & 0\end{bmatrix}$	$-\frac{X_{L_S}X_{P2}}{X_M}$

In general, to formulate an immittance network, at least three components are needed. The commonly used T-network and Π-network are depicted in Fig. 4(a) and (b). They feature the characteristics of immittance networks if the corresponding reactances satisfy

$$X_1 = X_2 = -X_3. \tag{24}$$

Equation (24) implies that the amplitudes of reactances in all branches are identical. If X_1 and X_2 are inductive, X_3 should be capacitive, and vice versa.

In addition to the three-component immittance networks, four-branch topologies are studied, as shown in Fig. 4(c)–(f). They are termed as Ladder Circuit 1, Ladder Circuit 2, Bridge-T circuit, and Lattice Circuit. As usual, X_i $(i = 1, 2, 3, 4)$ represents a generic reactance and the subscript i donates the numbers. The transmission parameters for the topologies can be derived. By making the transmission matrix satisfy (1), the design of the reactances is summarized in Table III. The characteristic impedance of the immittance resonant network is represented by $Z_{0,\mathrm{CLA}}$.

Authorized licensed use limited to: SOUTH CHINA UNIVERSITY OF TECHNOLOGY. Downloaded on May 14,2024 at 07:30:27 UTC from IEEE Xplore. Restrictions apply.

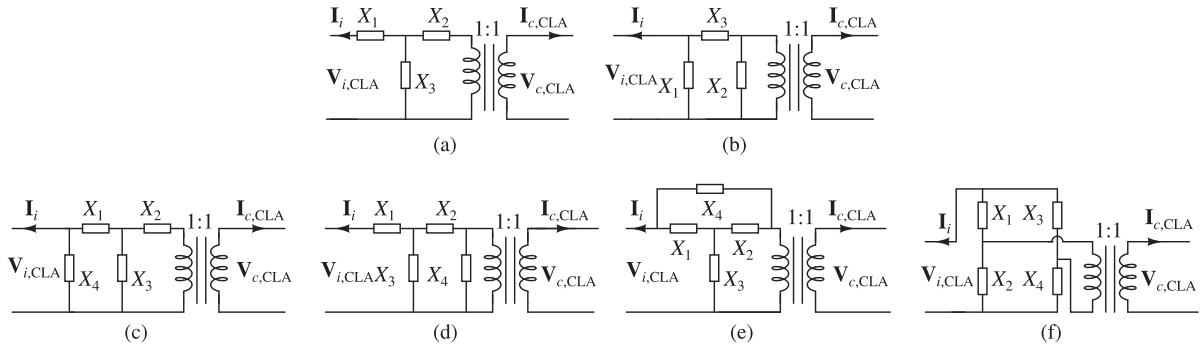

Fig. 4. Available clamping immittance networks with isolation. (a) T circuit. (b) Π circuit. (c) Ladder circuit1. (d) Ladder circuit2. (e) Bridge-T circuit. (f) Lattice circuit.

TABLE III
IMMITTANCE RESONANT NETWORKS OF CLAMPING IMMITTANCE NETWORKS

Topologies	Compensation design	A	$Z_{0,\mathrm{CLA}}$
T circuit	$X_1 = X_2 = -X_3$	$\begin{bmatrix} 0 & jX_3 \\ -\frac{1}{jX_3} & 0 \end{bmatrix}$	X_3
Π circuit	$X_1 = X_2 = -X_3$	$\begin{bmatrix} 0 & jX_3 \\ -\frac{1}{jX_3} & 0 \end{bmatrix}$	X_3
Ladder circuit 1	$X_1 = -X_3; X_4 = \frac{{X_3}^2}{X_2+X_3}$	$\begin{bmatrix} 0 & -jX_3 \\ \frac{1}{jX_3} & 0 \end{bmatrix}$	$-X_3$
Ladder circuit 2	$X_2 = -X_3; X_4 = \frac{{X_3}^2}{X_1+X_3}$	$\begin{bmatrix} 0 & -jX_3 \\ \frac{1}{jX_3} & 0 \end{bmatrix}$	$-X_3$
Bridge-T circuit	$X_1 = X_2; X_4 = -X_3(\frac{2+\frac{X_1}{X_3}}{1+\frac{X_3}{X_1}})$	$\begin{bmatrix} 0 & -j(2X_3+X_1) \\ \frac{1}{j(2X_3+X_1)} & 0 \end{bmatrix}$	$-(2X_3+X_1)$
Lattice circuit	S1: $X_1 = -X_3, X_2 = X_3$; S2: $X_1 = X_4 = -X_3$; S3: $X_2 = X_3, X_4 = -X_3$; S4: $X_2 = -X_1, X_4 = X_1$	S1-3: $\begin{bmatrix} 0 & -jX_3 \\ \frac{1}{jX_3} & 0 \end{bmatrix}$ S4: $\begin{bmatrix} 0 & jX_1 \\ -\frac{1}{jX_1} & 0 \end{bmatrix}$	S1-3: $-X_3$ S4: X_1

C. Configurable Output Current and Output Voltage

During the CC charging, output current $\mathbf{I}_{o,\mathrm{IPT}}$ of the secondary compensation circuit is inversely proportional to the characteristic impedance $Z_{0,\mathrm{IPT}}$ of the IPT immittance network at a constant input voltage of the primary compensation circuit, as shown in (13). Thus, by designing corresponding parameters of the loosely coupled transformer and compensation circuits that affect $Z_{0,\mathrm{IPT}}$, as given in Table II, various output currents can be configured to comply with different CC charging specifications.

The output voltage $\mathbf{V}_{o,\mathrm{IPT}}$ of the secondary compensation circuit is proportional to the ratio of the characteristic impedance $Z_{0,\mathrm{IPT}}$ of the IPT immittance network and inversely proportional to the characteristic impedance $Z_{0,\mathrm{CLA}}$ of the clamping immittance circuit, while $\mathbf{V}_{c,\mathrm{CLA}}$ of the clamping immittance network remains unchanged, according to (19). Once the CC output is configured via the design of $Z_{0,\mathrm{CLA}}$, the requirements of CV output can be configured by designing $Z_{0,\mathrm{CLA}}$. Considering there may exist practical limitations on the design of $Z_{0,\mathrm{CLA}}$, it is an alternative way to modify the CV output by varying the turn ratio of the isolated transformer, while keeping $Z_{0,\mathrm{CLA}}$ unchanged. Given an arbitrary turn ratio n of the isolated transformer, the secondary port of the IPT immittance network is derived in (19) can be modified as

$$\mathbf{V}_{o,\mathrm{IPT}} = n\frac{Z_{0,\mathrm{IPT}}}{Z_{0,\mathrm{CLA}}}\mathbf{V}_{c,\mathrm{CLA,max}}. \tag{25}$$

IV. EXPERIMENTAL VERIFICATION

To validate the synthesis of IPT converters with dual immittance networks for inherent CC-to-CV charging profiles, two sets of experimental prototypes are built. Key parameters are summarized in Table IV. The first prototype adopts the simplest configuration, which means series–series compensation for the IPT network and T circuit for the clamping network. The second prototype uses higher order resonant circuits, i.e., SP-PS compensation for the IPT network and Ladder Circuit 1 for the clamping network. Parameters for the IPT network and the clamping network are given in Table IV. A 48-V dc voltage source chopped by a full-bridge inverter is used to drive the IPT converters and an electronic load is used to emulate the battery.

Authorized licensed use limited to: SOUTH CHINA UNIVERSITY OF TECHNOLOGY. Downloaded on May 14,2024 at 07:30:27 UTC from IEEE Xplore. Restrictions apply.

TABLE IV
PARAMETERS OF EXPERIMENTAL PROTOTYPES

Parameters	Symbols	Measured values
Input voltage	$V_{\rm IN}$	48 V
Inverter switches	Q_1-Q_4	IRF640
Diodes	D_1-D_4	MBR20200
Equivalent load resistance	$R_{\rm eq}$	2 Ω to 80 Ω
Operating frequency	$\omega/2\pi$	85 kHz
S-S compensation	L_P, M, L_S	101.7 μH, 29.2 μH, 92.1 μH
	X_{P_1}, X_{S_1}	34.5 nF, 37.7 nF
Air gap distance	g_1	40 mm
Board inner diameter	d_i	117 mm
Board outer diameter	d_o	200 mm
Primary turns	N_P	21
Secondary turns	N_S	20
Litz wire	Φ_1	1.1 mm
T circuit	X_1, X_2, X_3	120.6 nF, 120.6 nF, 29.2 μH
SP-PS compensation	L_P, M, L_S	20 μH, 12.9 μH, 23 μH
	X_{P1}, X_{P2}	20 μH, 167 nF
	X_{S1}, X_{S2}	152 nF, 23 μH
Air gap distance	g_2	20 mm
Board Inner diameter	d_i	40 mm
Board Outer diameter	d_o	200 mm
Primary turn number	N_P	16
Secondary turn number	N_S	17
Lize wire	Φ_2	2.1 mm
Ladder circuit 1	X_1, X_2	25.2 μH, 14.8 μH
	X_3, X_4	140 nF, 49.5 μH

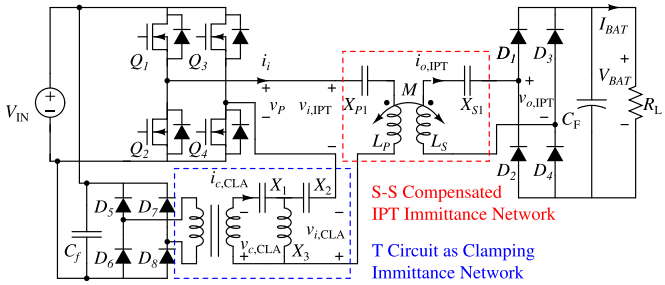

(a)

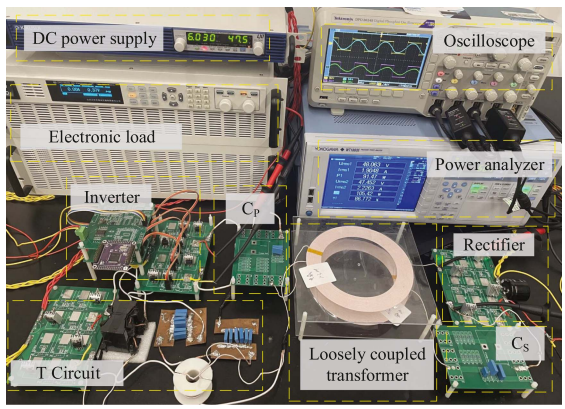

(b)

Fig. 5. Proposed IPT charging system including S-S compensated IPT immittance network and T circuit clamping immittance network. (a) Circuit diagram. (b) Experimental prototype.

A. S-S Compensated IPT Immittance Network with T Circuit as Clamping Immittance Network

In the experimental prototype shown in Fig. 5, the IPT converter includes an S-S compensated IPT immittance network, which works in conjunction with a T circuit clamping immittance network. The operating waveforms are shown in Fig. 6. The load conditions are set as $R_L = 5\,\Omega$, $R_L = 25\,\Omega$, and $R_L = 80\,\Omega$, which indicates the CC, transition, and CV modes, respectively. Since there are seven signals in total, two four-channel oscilloscopes were used to capture the waveforms simultaneously to better demonstrate CC and CV modes. v_P, i_i, and $v_{o,\rm IPT}$ are the ac input voltage, input current, and output voltage of the IPT immittance network, respectively. $v_{c,\rm CLA}$ and $i_{c,\rm CLA}$ are the ac input voltage and input current of the clamping immittance network, respectively. The dc output current and output voltage are labeled as $I_{\rm BAT}$ and $V_{\rm BAT}$, respectively. In the CC mode, $i_{c,\rm CLA}$ is zero, as shown in Fig. 6(a), and diodes D_1–D_4 of the assistive rectifier are reverse biased and the clamping immittance circuit does not operate, at which point the IPT immittance network operates as a conventional S-S compensated IPT converter to achieve the CC output. During CC-to-CV transition, as shown in Fig. 6(b), the assistive rectifier is activated early because of the partial conduction of D_1–D_4. Since $i_{c,\rm CLA}$ is still small, the rectifier works in discontinuous conduction mode. In the late CV mode, as shown in Fig. 6(c), i_i is clamped to achieve the CV output because the clamping immittance network is fully conducted. Furthermore, the output voltage is almost independent of the load. Throughout the charging process, $v_{i,\rm IPT}$ and i_i remain in phase, verifying that the unity power factor has been achieved and ensuring that the low reactive power in the circuit will be minimized.

The measured $I_{\rm BAT}$ (marked with"◯") and $V_{\rm BAT}$ (marked with "□") versus R_L are plotted in Fig. 7. An approximate CC output at 2.5 A can be achieved when $R_L \le 15\ \Omega$, while an approximate CV threshold at 51 V is maintained if $R_L \ge 26\ \Omega$. Nevertheless, the required inherent CC-to-CV transition can be achieved in a short load range. The measured efficiency η (marked with "△") versus R_L is also plotted in Fig. 7. A maximum efficiency of 88.3% is achieved at 15 Ω. At the CC stage, the clamping immittance circuit is not activated ($i_{c,\rm CLA} = 0$), and thus, no power loss is incurred by the clamping immittance circuit. In the CC-to-CV transition process and early CV stage, due to $i_{c,\rm CLA} \approx 0$, the efficiency is not affected too much by the power losses incurred by the clamping immittance circuit. At the late CV stage (light-load conditions), power losses incurred by the clamping immittance circuit become significant as $i_{c,\rm CLA}$ increases with the decrease of output power. It is acceptable that a penalty in efficiency caused by the use of the clamping immittance circuit only occurs in light-load conditions.

Transient waveforms for step change in load are shown in Fig. 8. The primary current i_i, output voltage $V_{\rm BAT}$, and output current $I_{\rm BAT}$ are presented. The load resistance is step changed from 8 to 40 Ω and from 40 to 60 Ω. When $R_L = 8\,\Omega$, the magnitude of i_i is smaller than its maximum value 4.8 A, and thus, the IPT converter operates as a CC charger. When R_L is step changed to 40 and 60 Ω, the magnitude of i_i is tightly limited to its maximum value 4.8 A, and $V_{\rm BAT}$

Authorized licensed use limited to: SOUTH CHINA UNIVERSITY OF TECHNOLOGY. Downloaded on May 14,2024 at 07:30:27 UTC from IEEE Xplore. Restrictions apply.

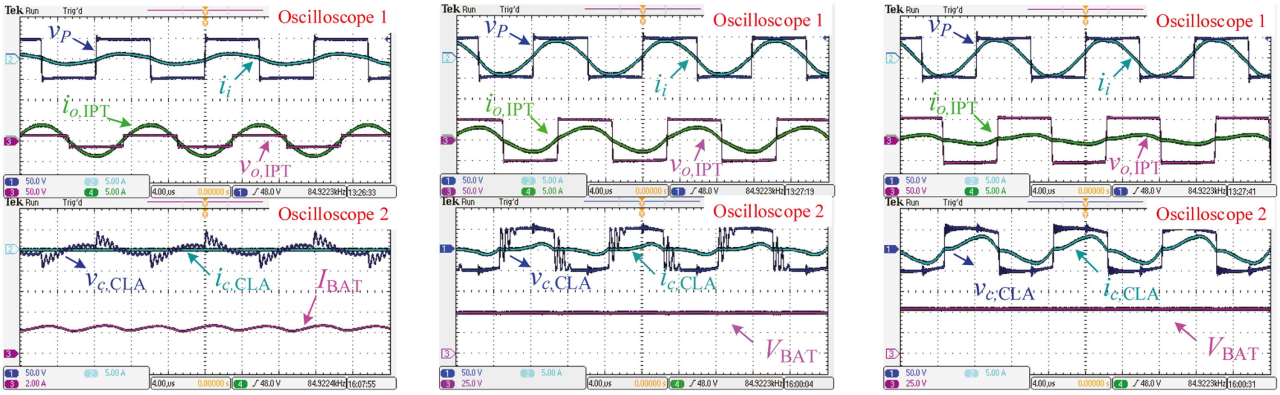

Fig. 6. Captured operating waveforms of experimental prototype with S-S compensation as the IPT network and T circuit as the clamping network. (a) CC mode, $R_L = 5\,\Omega$. (b) Transition process, $R_L = 25\,\Omega$. (c) CV mode, $R_L = 80\,\Omega$.

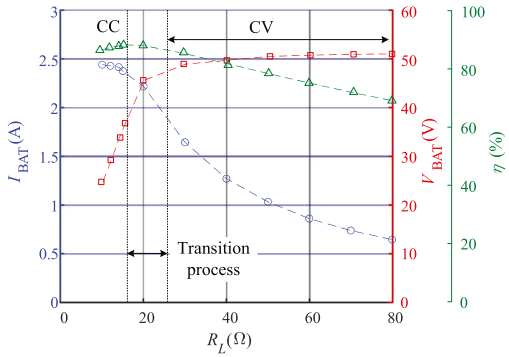

Fig. 7. Measured DC output current I_{BAT}, DC output voltage V_{BAT}, and power efficiency η versus load resistance R_L of the experimental prototype with S-S compensation as the IPT network and T circuit as the clamping network.

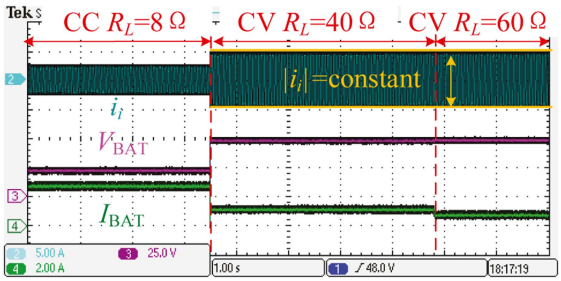

Fig. 8. Transient waveforms for R_L step changing from 8 to 40 Ω and from 40 to 60 Ω of the experimental prototype with S-S compensation as the IPT network and T circuit as the clamping network.

is tightly limited to a threshold value 51 V, as shown in Fig. 8.

B. SP-PS Compensated IPT Immittance Network with Ladder Circuit 1 as Clamping Immittance Network

In the experimental prototype shown in Fig. 9, the IPT converter includes an SP-PS compensated IPT immittance network that works in conjunction with a Ladder circuit 1 clamping immittance network. The operating waveforms are shown in Fig. 10. The load conditions are set as $R_L = 10\,\Omega$, $R_L = 25\,\Omega$,

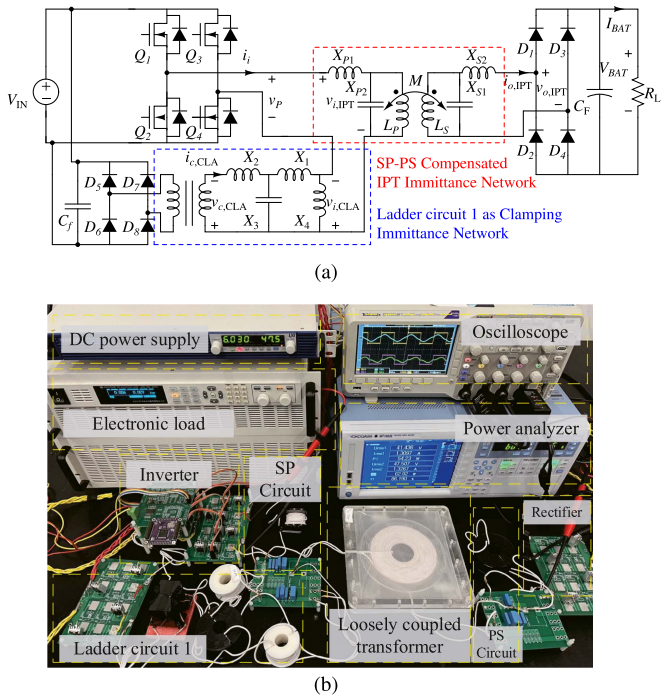

Fig. 9. Proposed IPT charging system including SP-PS compensated IPT immittance network and Ladder circuit 1 clamping immittance network. (a) Circuit diagram. (b) Experimental prototype.

and $R_L = 80\,\Omega$, which indicates the CC, transition, and CV modes, respectively. Since there are seven signals in total, two four-channel oscilloscopes were used to capture the waveforms simultaneously to better demonstrate CC and CV modes. v_P, i_i, and $v_{o,\mathrm{IPT}}$ are the ac input voltage, input current, and output voltage of the IPT immittance network, respectively. $v_{c,\mathrm{CLA}}$ and $i_{c,\mathrm{CLA}}$ are the ac input voltage and input current of the clamping immittance network, respectively. The dc output current and output voltage are labeled as I_{BAT} and V_{BAT}, respectively. In the CC mode, $i_{c,\mathrm{CLA}}$ is zero, as shown in Fig. 10(a), diodes D_1–D_4 of the assistive rectifier are reverse biased, and the clamping immittance circuit does not operate, at which point the IPT immittance network operates as a conventional

Authorized licensed use limited to: SOUTH CHINA UNIVERSITY OF TECHNOLOGY. Downloaded on May 14,2024 at 07:30:27 UTC from IEEE Xplore. Restrictions apply.

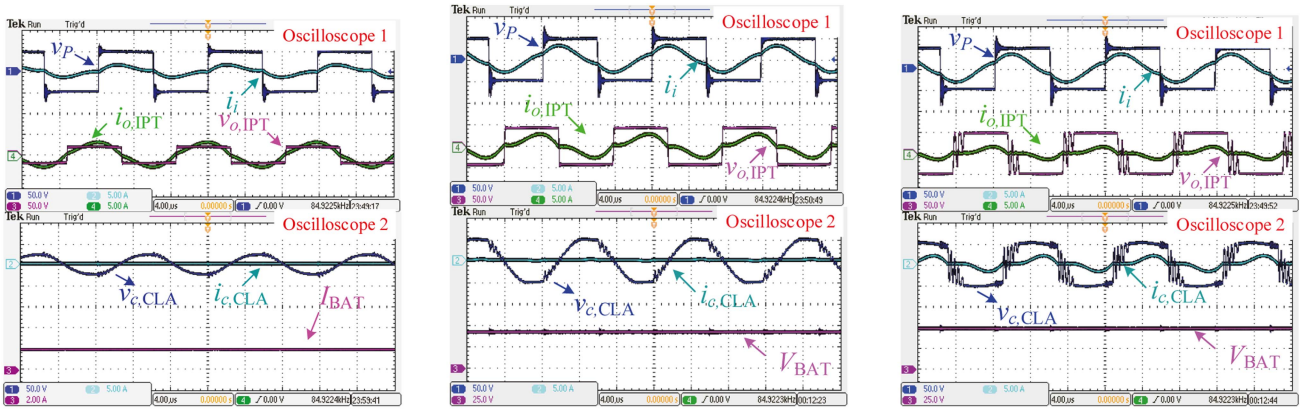

Fig. 10. Captured operating waveforms of experimental prototype with SP-PS compensation as the IPT network and Ladder circuit 1 as the clamping network. (a) CC mode, $R_L = 10\,\Omega$. (b) Transition process, $R_L = 25\,\Omega$. (c) CV mode, $R_L = 80\,\Omega$.

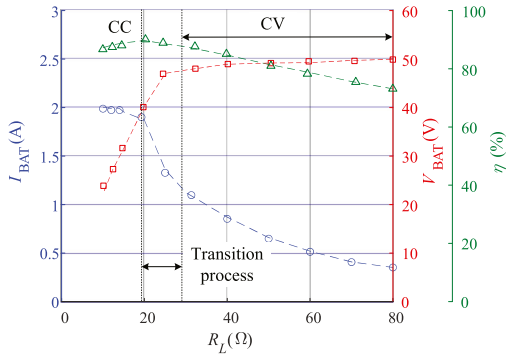

Fig. 11. Measured DC output current I_{BAT}, DC output voltage V_{BAT}, and power efficiency η versus load resistance R_L of the experimental prototype with SP-PS compensation as the IPT network and Ladder circuit 1 as the clamping network.

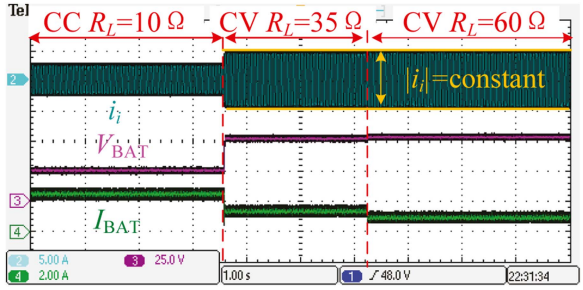

Fig. 12. Transient waveforms for R_L step changing from 10 to 35 Ω and from 35 to 60 Ω of the experimental prototype with SP-PS compensation as the IPT network and Ladder circuit 1 as the clamping network.

SP-PS compensated IPT converter to achieve the CC output. During CC-to-CV transition, as shown in Fig. 10(b), the assistive rectifier is activated early because of the partial conduction of D_1–D_4. Since $i_{c,\mathrm{CLA}}$ is still small, the rectifier works in discontinuous conduction mode. In the late CV mode, as shown in Fig. 10(c), i_i is clamped to achieve the CV output because the clamping immittance network is fully conducted. Furthermore, the output voltage is almost independent of the load. Throughout the charging process, $v_{i,\mathrm{IPT}}$ and i_i remain in phase, verifying that the unity power factor has been achieved and ensuring that the low reactive power in the circuit will be minimized.

The measured I_{BAT} (marked with"◯") and V_{BAT} (marked with "□") versus R_L are plotted in Fig. 11. An approximate CC output at 2 A can be achieved when $R_L \leq 19\ \Omega$, while an approximate CV threshold at 50 V is maintained if $R_L \geq 28\ \Omega$. Nevertheless, the required inherent CC-to-CV transition can be achieved in a short load range. The measured efficiency η (marked with "△") versus R_L is also plotted in Fig. 11. A maximum efficiency of 88.1% is achieved at 19 Ω. At the CC stage, the clamping immittance circuit is not activated ($i_{c,\mathrm{CLA}} = 0$), and thus, no power loss is incurred by the clamping immittance circuit. In the CC-to-CV transition process and early CV stage, due to $i_{c,\mathrm{CLA}} \approx 0$, the efficiency is not affected too much by the power losses incurred by the clamping immittance circuit. At the late CV stage (light-load conditions), power losses incurred by the clamping immittance circuit become significant as $i_{c,\mathrm{CLA}}$ increases with the decrease of output power. It is acceptable that a penalty in efficiency caused by the use of the clamping immittance circuit only occurs in light-load conditions.

Transient waveforms for step change in load are shown in Fig. 12. The primary current i_i, output voltage V_{BAT}, and output current I_{BAT} are presented. The load resistance is step changed from 10 to 35 Ω and from 35 to 60 Ω. When $R_L = 10\,\Omega$, the magnitude of $v_{i,\mathrm{IPT}}$ is smaller than its maximum value 4.7 A, and the IPT converter works as a CC charger. When R_L is step changed from 35 to 60 Ω, the magnitude of $v_{i,\mathrm{IPT}}$ is firmly constrained to its most maximum value 4.7 A, and V_{BAT} is firmly constrained to a threshold value 50 V, as shown in Fig. 12.

V. Conclusion

Traditional IPT systems used for battery charging often face challenges in achieving a seamless transition from CC to CV charging. These challenges include the need for additional control design, redundant topology structure, and complex parameter configuration. To overcome these challenges, we propose a systematic approach to design IPT charging systems that

Authorized licensed use limited to: SOUTH CHINA UNIVERSITY OF TECHNOLOGY. Downloaded on May 14,2024 at 07:30:27 UTC from IEEE Xplore. Restrictions apply.

simplify the control schemes, modularize the system structure, and improve the design freedom for parameter configuration based on the theory of immittance networks. By adding a clamping immittance network to the primary side of an IPT converter with characteristics of immittance networks, a family of the charging systems can be derived. The automatic CC-to-CV transition of an IPT charging system can be realized by clamping the primary side current of the IPT immittance network through a clamping immittance circuit. This passive solution allows the removal of state-of-charge detection and wireless communication, simplifying the corresponding control scheme significantly. The connection style of the dual immittance networks offers the possibility of power decoupling between the networks, thereby enables a modular structure and straightforward parameter configuration process. IPT resonant tanks and isolated resonant circuits, exhibiting characteristics of immittance networks, are analyzed and identified, facilitating the derivation and selection of dual-immittance-network IPT charging systems for various application scenarios. The proposed passive control solution offers high reliability, simplicity in secondary circuit design, and elimination of complex control algorithms. However, it should be noted that efficiency can still be further improved. Specifically, reducing power losses caused by mismatching load impedance and components in the clamping immittance network would enhance the performance of the proposed IPT system.

REFERENCES

[1] A. Kurs, A. Karalis, R. Moffatt, J. D. Joannopoulos, P. Fisher, and M. Soljacic, "Wireless power transfer via strongly coupled magnetic resonances," *Science*, vol. 317, no. 5834, pp. 83–86, Jul. 2007.

[2] X. Liu and S. Y. Hui, "Optimal design of a hybrid winding structure for planar contactless battery charing platform," *IEEE Trans. Power Electron.*, vol. 23, no. 1, pp. 455–463, Jan. 2008.

[3] S. Lee, B. Chao, and C. T. Rim, "Dynamics characterization of the inductive power transfer system for online electric vehicles by Laplace phasor transform," *IEEE Trans. Power Electron.*, vol. 28, no. 12, pp. 5902–5909, Dec. 2013.

[4] Z. Huang, S. C. Wong, and C. K. Tse, "Design of a single-stage inductive-power-transfer converter for efficient EV battery charging," *IEEE Trans. Veh. Technol.*, vol. 66, no. 7, pp. 5808–5821, Jul. 2017.

[5] V. Gupta, S. R. Konda, R. Kumar, and B. K. Panigrahi, "Electric vehicle driver response evaluation in multiaggregator charging management with EV routing," *IEEE Trans. Ind. Appl.*, vol. 56, no. 6, pp. 6914–6924, Nov./Dec. 2020.

[6] S. C. Tang, T. L. T. Lun, Z. Guo, K. Kwok, and N. J. McDannold, "Intermediate range wireless power transfer with segmented coil transmitters for implantable heart pumps," *IEEE Trans. Power Electron.*, vol. 32, no. 5, pp. 3844–3857, May 2017.

[7] Q. Chen, S. C. Wong, C. K. Tse, and X. Ruan, "Analysis, design and control of a transcutaneous power regulator for artificial hearts," *IEEE Trans. Biomed. Circ. Syst.*, vol. 3, no. 1, pp. 23–31, Feb. 2009.

[8] C. Xiao, D. Cheng, and K. Wei, "An LCC-C compensated wireless charging system for implantable cardiac pacemakers: Theory, experiment, and safety evaluation," *IEEE Trans. Power Electron.*, vol. 33, no. 6, pp. 4894–4905, Jun. 2018.

[9] S. Y. R. Hui, "Planar wireless charging technology for portable electronic products and Qi," *Proc. IEEE*, vol. 101, no. 6, pp. 1290–1301, Jun. 2013.

[10] B. Choi, J. Nho, H. Cha, T. Ahn, and S. Choi, "Design and implementation of low-profile contactless battery charger using planar printed circuit board windings as energy transfer device," *IEEE Trans. Ind. Electron.*, vol. 59, no. 1, pp. 140–147, Feb. 2004.

[11] A. A. Hussein and I. Batarseh, "A review of charging algorithms for nickel and lithium battery chargers," *IEEE Trans. Veh. Technol.*, vol. 60, no. 3, pp. 830–838, Mar. 2011.

[12] Z. Li, H. Liu, Y. Tian, and Y. Liu, "Constant current/voltage charging for primary-side controlled wireless charging system without using dual-side communication," *IEEE Trans. Power Electron.*, vol. 36, no. 12, pp. 13562–13577, Dec. 2021.

[13] K. Song, Z. Li, J. Jiang, and C. Zhu, "Constant current/voltage charging operation for series-series and series-parallel compensated wireless power transfer systems employing primary-side controller," *IEEE Trans. Power Electron.*, vol. 33, no. 9, pp. 8065–8080, Sep. 2018.

[14] H. Wu, S. C. Wong, C. K. Tse, S. Y. R. Hui, and Q. Chen, "Single-phase LED drivers with minimal power processing, constant output current, input power factor correction, and without electrolytic capacitor," *IEEE Trans. Power Electron.*, vol. 33, no. 7, pp. 6159–6170, Jul. 2018.

[15] M. Kim, D. M. Joo, B. K. Lee, and D. G. Woo, "Design and control of inductive power transfer system for electric vehicles considering wide variation of output voltage and coupling coefficient," *IEEE Trans. Power Electron.*, vol. 34, no. 2, pp. 1197–1208, Feb. 2019.

[16] K. Colak, E. Asa, M. Bojarski, D. Czarkowski, and O. C. Onar, "A novel phase-shift control of semibridgeless active rectifier for wireless power transfer," *IEEE Trans. Power Electron.*, vol. 30, no. 11, pp. 6288–6297, Nov. 2015.

[17] Z. Huang, D. Wang, and X. Qu, "A novel IPT converter with current-controlled semi-active rectifier for efficiency enhancement throughout supercapacitor charging process," *IEEE J. Emerg. Sel. Topics Power Electron.*, vol. 10, no. 2, pp. 2201–2209, Apr. 2022.

[18] Z. Huang, T. Qin, and H. H. C. Iu, "Primary-tuning wireless constant-current charger with self-sustained constant-voltage limit featuring minimal secondary design," *IEEE J. Emerg. Sel. Topics Power Electron.*, vol. 11, no. 5, pp. 5500–5508, Oct. 2023.

[19] V. B. Vu, D. H. Tran, and W. Choi, "Implementation of the constant current and constant voltage charge of inductive power transfer systems with the double-sided LCC compensation topology for electric vehicle battery charge applications," *IEEE Trans. Power Electron.*, vol. 33, no. 9, pp. 7398–7410, Sep. 2018.

[20] J. Lu, G. Zhu, D. Lin, Y. Zhang, J. Jiang, and C. C. Mi, "Unified load-independent ZPA analysis and design in CC and CV modes of higher order resonant circuits for WPT systems," *IEEE Trans. Transp. Electrific.*, vol. 5, no. 4, pp. 977–987, Dec. 2019.

[21] C. S. Wang, G. A. Covic, and O. H. Stielau, "Power transfer capability and bifurcation phenomena of loosely coupled inductive power transfer systems," *IEEE Trans. Ind. Electron.*, vol. 51, no. 1, pp. 148–157, Feb. 2004.

[22] J. Hou, Q. Chen, S. C. Wong, C. K. Tse, and X. Ruan, "Analysis and control of series/series-parallel compensated resonant converter for contactless power transfer," *IEEE Trans. Power Electron.*, vol. 3, no. 1, pp. 124–136, Mar. 2015.

[23] Y. Jiang, L. Wang, Y. Wang, J. Liu, M. Wu, and G. Ning, "Analysis, design, and implementation of WPT system for EV's battery charging based on optimal operation frequency range," *IEEE Trans. Power Electron.*, vol. 34, no. 7, pp. 6890–6905, Jul. 2019.

[24] J. Hou, Q. Chen, L. Zhang, L. Xu, S. C. Wong, and C. K. Tse, "Compact capacitive compensation for adjustable load-independent output and zero-phase-angle input for high efficiency IPT systems," *IEEE J. Emerg. Sel. Topics Power Electron.*, vol. 10, no. 4, pp. 4923–4936, Aug. 2022.

[25] S. Li, W. Li, J. Deng, T. D. Nguyen, and C. Mi, "A double-sided LCC compensation network and its tuning method for wireless power transfer," *IEEE Trans. Veh. Technol.*, vol. 64, no. 6, pp. 2261–2273, Jun. 2015.

[26] X. Qu, Y. Jing, H. Han, S. C. Wong, and C. K. Tse, "Higher order compensation for inductive-power-transfer converters with constant-voltage or constant-current output combating transformer parameter constraints," *IEEE Trans. Power Electron.*, vol. 32, no. 1, pp. 394–405, Jan. 20176.

[27] J. Hou, Q. Chen, Z. Zhang, S. C. Wong, and C. K. Tse, "Analysis of output current characteristics for higher order primary compensation in inductive power transfer systems," *IEEE Trans. Power Electron.*, vol. 33, no. 8, pp. 6807–6821, Aug. 2018.

[28] X. Qu, H. Han, S. C. Wong, C. K. Tse, and W. Chen, "Hybrid IPT topologies with constant current or constant voltage output for battery charging applications," *IEEE Trans. Power Electron.*, vol. 30, no. 11, pp. 6329–6337, Nov. 2015.

[29] Y. Chen, B. Yang, Z. Kou, Z. He, G. Cao, and R. Mai, "Hybrid and reconfigurable IPT systems with high-misalignment tolerance for constant-current and constant-voltage battery charging," *IEEE Trans. Power Electron.*, vol. 33, no. 10, pp. 8259–8269, Oct. 2018.

[30] Y. Li et al., "Reconfigurable intermediate resonant circuit based WPT system with load-independent constant output current and voltage for charging battery," *IEEE Trans. Power Electron.*, vol. 34, no. 3, pp. 1988–1992, Mar. 2019.

Authorized licensed use limited to: SOUTH CHINA UNIVERSITY OF TECHNOLOGY. Downloaded on May 14,2024 at 07:30:27 UTC from IEEE Xplore. Restrictions apply.

[31] B. Cheng and L. He, "High-order network based general modeling method for improved transfer performance of the WPT system," *IEEE Trans. Power Electron.*, vol. 36, no. 11, pp. 12375–12388, Nov. 2021.
[32] X. Mao, J. Chen, Y. Zhang, and J. Dong, "A simple and reconfigurable wireless power transfer system with constant voltage and constant current charging," *IEEE Trans. Power Electron.*, vol. 37, no. 5, pp. 4921–4925, May 2022.
[33] M. Borage, K. V. Nagesh, M. S. Bhatia, and S. Tiwari, "Resonant immittance converter topologies," *IEEE Trans. Power Electron.*, vol. 58, no. 3, pp. 971–978, Mar. 2011.
[34] L. Cao, J. Lin, X. Jiang, C. S. Wong, and K. H. Loo, "An immittance-network-based multiport ZVS bidirectional converter with power decoupling capability," *IEEE Trans. Power Electron.*, vol. 37, no. 10, pp. 12729–12740, Oct. 2022.
[35] Z. Huang, S. C. Wong, and C. K. Tse, "Comparison of basic inductive power transfer systems with linear control achieving optimized efficiency," *IEEE Trans. Power Electron.*, vol. 35, no. 3, pp. 3276–3286, Mar. 2020.

Zhicong Huang (Senior Member, IEEE) received the B.Eng. degree in electrical engineering and automation and the M.Eng. degree in mechanical and electronic engineering from the Huazhong University of Science and Technology, Wuhan, China, in 2010 and 2013, respectively, and the Ph.D. degree in power electronics from The Hong Kong Polytechnic University, Hong Kong, in 2018.

He is currently an Associate Professor with the Shien-Ming Wu School of Intelligent Engineering, South China University of Technology, Guangzhou, China. His research interests include power electronics techniques in electric vehicles and power systems.

Dr. Huang was the recipient of the Outstanding Reviewer Award from IEEE TRANSACTION ON POWER ELECTRONICS in 2021.

Tian Qin (Student Member, IEEE) was born in Wuhan, China, in 1998. She received the B.Eng. degree in electrical engineering and automation from the Hubei University of Technology, Wuhan, China, in 2021. She is currently working toward the M.Eng. degree in intelligent engineering with the Shien-Ming Wu School of Intelligent Engineering, South China University of Technology, Guangzhou, China.

Her current research focuses on wireless power transfer.

Xiaolu Lucia Li (Member, IEEE) received the B.Eng. and M.Phil. degrees in electrical engineering from the Harbin Institute of Technology, Harbin, China, in 2014 and 2016, respectively, and the Ph.D. degree in power electronics from Hong Kong Polytechnic University, Hong Kong, in 2019.

She is currently a Postdoctoral Fellow with the Department of Electrical Engineering, City University of Hong Kong. Her research interests include multiport converters and wireless power transfer.

Li Ding (Member IEEE) received the B.E. degree in information engineering from the Guangdong University of Technology, Guangzhou, China, in 2011, the M.E. degree in signal and information processing from South China University of Technology, Guangzhou, in 2014, and the Ph.D. degree in power electronics from The Hong Kong Polytechnic University, Hong Kong, in 2022.

He is currently a Postdoctoral Researcher with the Department of Electrical Engineering, City University of Hong Kong, Hong Kong. His research interests include modeling and analysis of power electronic systems, and study the complex behavior in power electronic circuits.

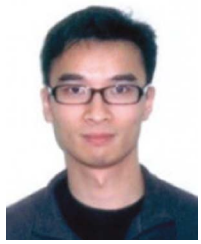

Herbert Ho-Ching Iu (Senior Member, IEEE) received the B.Eng. (Hons.) degree in electrical and electronic engineering from the University of Hong Kong, Hong Kong, in 1997, and the Ph.D. degree in power electronics from the Hong Kong Polytechnic University, Hong Kong, in 2000.

In 2002, as a Lecturer, he joined the School of Electrical, Electronic, and Computer Engineering, The University of Western Australia, where he is currently a Professor. He has authored or coauthored 150 papers in the areas of his research fields, and he is a Co-Editor of *Control of Chaos in Nonlinear Circuits and Systems* (World Scientific, 2009) and a coauthor of *Development of Memristor Based Circuits* (World Scientific, 2013). His research interests include power electronics, renewable energy, nonlinear dynamics, current sensing techniques, and memristive systems.

Dr. Ho-Ching Iu was the recipient of two IET Premium Awards in 2012 and 2014, UWA Vice-Chancellor's Mid-Career Research Award in 2014, 2023 IEEE TRANSACTIONS ON CIRCUITS AND SYSTEMS Guillemin-Cauer Best Paper Award, 2021 IEEE JOURNAL OF EMERGING AND SELECTED TOPICS in Power Electronics Prize Paper Award, 2019 IEEE TRANSACTIONS ON VERY LARGE SCALE INTEGRATION SYSTEMS Prize Paper Award, and Best Paper Award of 2019 IEEE International Conference on Artificial Intelligence Circuits and Systems. He is currently an Editor-in-Chief of IEEE JOURNAL ON SELECTED AND EMERGING TOPICS IN CIRCUITS AND SYSTEMS, Associate Editor for IEEE TRANSACTIONS ON CIRCUITS AND SYSTEMS II, IEEE TRANSACTIONS ON POWER ELECTRONICS, IEEE JOURNAL OF EMERGING AND SELECTED TOPICS ON POWER ELECTRONICS, and IEEE TRANSACTIONS ON SMART GRID. He was appointed as IEEE CASS Distinguished Lecturer for 2023–2024.

Chi K. Tse (Fellow, IEEE) received the B.Eng. (Hons) degree and the Ph.D. degree in electrical engineering from the University of Melbourne, Parkville, VIC, Australia, in 1987 and 1991, respectively.

He is currently the Associate Vice President (Innovation) and Chair Professor of electrical engineering with City University of Hong Kong, Hong Kong. His research interests include power electronics, nonlinear circuits, and complex network applications.

Authorized licensed use limited to: SOUTH CHINA UNIVERSITY OF TECHNOLOGY. Downloaded on May 14,2024 at 07:30:27 UTC from IEEE Xplore. Restrictions apply.